Contribution of double scattering to structural coloration in quasiordered nanostructures of bird feathers

Heeso Noh,[1] Seng Fatt Liew,[1] Vinodkumar Saranathan,[2] Richard O. Prum,[2] Simon G. J. Mochrie,[1,3] Eric R. Dufresne,[3,4,5] and Hui Cao[1,3]

[1]*Department of Applied Physics, Yale University, New Haven, Connecticut 06511, USA*

[2]*Department of Ecology and Evolutionary Biology and Peabody National History Museum, Yale University, New Haven, Connecticut 06511, USA*

[3]*Department of Physics, Yale University, New Haven, Connecticut 06511, USA*

[4]*Department of Mechanical Engineering, Yale University, New Haven, Connecticut 06511, USA*

[5]*Department of Chemical Engineering, Yale University, New Haven, Connecticut 06511, USA*

(Received 17 September 2009; revised manuscript received 2 April 2010; published 25 May 2010)

We measured the polarization- and angle-resolved optical scattering and reflection spectra of the quasiordered nanostructures in the bird feather barbs. In addition to the primary peak that originates from single scattering, we observed a secondary peak which exhibits depolarization and distinct angular dispersion. We explained the secondary peak in terms of double scattering, i.e., light is scattered successively twice by the structure. The two sequential single-scattering events are considered uncorrelated. Using the Fourier power spectra of the nanostructures obtained from the small-angle x-ray scattering experiment, we calculated the double scattering of light in various directions. The double-scattering spectrum is broader than the single-scattering spectrum, and it splits into two subpeaks at larger scattering angle. The good agreement between the simulation results and the experimental data confirms that double scattering of light makes a significant contribution to the structural color.

DOI: 10.1103/PhysRevE.81.051923 PACS number(s): 42.66.−p, 42.25.−p, 87.85.J−

I. INTRODUCTION

Over the past decade there have been revived interests in structural coloration in nature, partly due to rapid developments of artificial photonic materials such as photonic crystals [1]. The structural coloration originates from light scattering by nanoscale variation of refractive index in biological structures. Constructive interference of light scattered by periodic structures produces iridescent colors [2–5]. Recent studies showed that quasiordered nanostructures, which are isotropic and have short-range order, can generate noniridescent colors with omnidirectional lighting [4,6–13]. Prum *et al.* were able to predict the optical reflectance spectra via Fourier analysis of such structures in the bird feather barbs. The prediction is based on the assumption of single scattering, i.e., light is scattered only once by the structure. The Fourier spectrum of the structure reveals the existence of a dominant length scale for structural correlation, which results in one peak in the predicted reflectance spectrum. The measured reflectance spectra of many bird feathers, however, exhibit two peaks [11]. A comparison of the small-angle x-ray scattering (SAXS) data to the optical measurements also showed significant differences for some bird feathers [12]. The SAXS directly measures the spatial Fourier spectra of structures because it involves only single-scattering process. The primary peak in the optical reflectance spectrum coincides with the SAXS peak, confirming it originates from single scattering of light. There is a secondary peak in the optical reflectance spectrum, which does not correspond to any SAXS peak. This result implies the origin of the secondary peak may be multiple scattering. However, the general belief is that multiple scattering simply broadens the single-scattering peak instead of producing additional peaks in the spectrum. This is because the incident angle of light is randomized during the repetitive scattering by the quasiordered structure [14,15]. For a fixed observation direction, the single scattering peak shifts in frequency as the incident angle varies, thus the average of the single-scattering spectrum over all possible incident angles produces a spectrally broad peak for multiple scattering.

The secondary peak plays an important role in the structural coloration of feather barbs of many bird species. One example is the vivid turquoise-blue plumage of the plum-throated Cotinga (*Cotinga Maynana*). The turquoise color corresponds to the primary peak in the reflectance spectrum, and the blue color to the secondary peak. Although the secondary peak appears frequently in bird feathers, there has been no detailed study of it. It is not known whether and how the secondary peak changes with the viewing angle and the orientation of feather barbs, what its polarization is and how it is related to that of incident light.

In this paper, we identify the physical origin of the secondary peak via experimental and theoretical studies of optical scattering spectra of quasiordered nanostructures of bird feathers. We performed polarization- and angle-resolved reflection and scattering spectrometry on feather barbs. While the primary peak in the reflection and scattering spectrum maintains the polarization of the incident white light, the secondary peak acquires a cross-polarization component. The depolarization of the secondary peak indicates it originates from multiple scattering of light. Near the backscattering direction, the secondary peak has shorter wavelength than the primary peak. As the angle θ between the line of sight and that of illumination increases, the secondary peak shifts to longer wavelength while the primary peak to shorter wavelength. We explained the secondary peak by double

scattering, i.e., light is scattered successively twice by the structure. The two sequential single-scattering events are regarded as independent. Using the structural information obtained from the SAXS data, we calculated the double-scattering spectra for different angle θ. The short-range structural correlation produces a broad peak in the double-scattering spectra, which splits into two subpeaks with increasing θ. The subpeak at longer wavelength redshifts as θ increases. Its angular dispersion agrees to that of the secondary peak observed experimentally, confirming the secondary peak originates from double scattering of light.

The paper is organized as follows. We start with the structural characterization of bird feather barbs in Sec. II, followed by a description of the optical measurement setups in Sec. III. Sections IV and V present the experimental data of polarization and directional prosperities of scattered and reflected light. Section VI details our calculation and analysis of single scattering, followed by those of the double scattering in Sec. VII. Section VIII is the conclusion.

II. STRUCTURAL CHARACTERIZATION

Structural colors are produced by the spongy β-keratin and air nanostructures within the medullary cells of bird feather barb rami [6,7,16,17]. Known barb nanostructures belong to two distinct morphological classes [4,8]. Channel-type nanostructures consist of β-keratin bars and air channels in elongate, tortuous, and twisting forms. Sphere-type nanostructures consist of highly spherical air cavities that are surrounded by thin β-keratin bars and sometimes interconnected by tiny passages. Our previous studies suggest these nanostructures are self-assembled during phase separation of β-keratin protein from the cytoplasm of the cell [12,18]. The channel morphology is developed via spinodal decomposition [19], while the spherical morphology via nucleation and growth.

We studied feather barbs of six bird species, three with channel-type structures, and three sphere type. Their optical measurement results as well as SAXS data are similar. In the following we present the data for *Cotinga maynana* (*C. maynana*) which has the sphere-type nanostructure.

To characterize the nanostructures *in situ*, we measured SAXS of feather barbs. SAXS directly gives the power Fourier transform of the structure via single scattering, without complications from multiple scattering. The SAXS data were collected at beam line 8-ID-I at the Advanced Photon Source at Argonne National Laboratories. The x-ray wavelength is 1.68 Å. As shown in the inset of Fig. 1(a), the SAXS pattern of *C. maynana* feather barbs exhibits rings, indicating the underlying nanostructures are isotropic. Exploiting the rotation symmetry, we averaged the scattered x-ray intensity over the azimuthal angle to obtain the intensity I as a function of spatial frequency q [Fig. 1(a)]. $I(q)$ has a primary peak at $q_0=0.03$ nm^{-1}, revealing the existence of a dominant length scale for structural correlation. From q_0 we deduced the correlation length $s=2\pi/q_0=208$ nm, which is about half of the wavelength of blue light. $I(q)$ has a much weaker

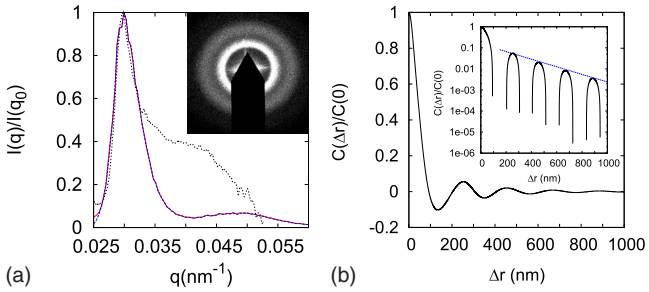

FIG. 1. (Color online) (a) Inset: small-angle x-ray scattering (SAXS) pattern from the *C. maynana* feather barbs. Main panel: red solid curve is the azimuthal average of SAXS intensity $I(q)$ normalized to the maximal value $I(q_0)$. The blue dashed curve is the fitted $I(q)$ for smaller q to eliminate the artificial signal from x-ray diffraction by the beam block. The black dotted curve is the optical scattering intensity plotted against q for $\theta=10°$ (see text). (b) Spatial correlation function $C(\Delta r)$ obtained from the Fourier transform of $I(q)$, normalized to $C(\Delta r=0)$. Inset is a log-linear plot which shows the exponential decay of $C(\Delta r)$ with Δr.

second peak at higher spatial frequency 0.049 nm^{-1}. It corresponds to a correlation length of 128 nm, which is significantly smaller than the optical wavelength.

The full width at half maximum (FWHM) Δq of the primary peak in $I(q)$ reflects the range ξ of spatial order. For *C. maynana* $\xi=2\pi/\Delta q=1.24$ μm. Since ξ is only six times of spatial period s, the order is short ranged. We also Fourier transformed the SAXS pattern to obtain the spatial correlation function $C(\Delta r)$ of nanostructures. As shown in Fig. 1(b), the amplitude of $C(\Delta r)$ decays quickly with spatial separation Δr. The log-linear plot illustrates the envelop of $C(\Delta r)$ decays exponentially with Δr. This result confirms the nanostructure has only short-range order.

III. OPTICAL SETUPS

We conducted polarization- and angle-resolved reflection and scattering spectrometry on the feather barbs. A bird feather is mounted at the rotation center of a goniometer. Collimated white light from a UV-enhanced Xe lamp is incident on the sample at an angle ϕ from the surface normal. The spot size on the sample is about 1 mm. Reflected or scattered light is collected by a lens and focused to an optical fiber that is connected to a spectrometer (Ocean Optics HR2000+). The spectral resolution is 1.5 nm. The angular resolution, which is determined mainly by the collection angle of the lens, is about 5°. In the polarization experiment, one linear polarizer is placed in the path of incident white light, and another linear polarizer is placed in front of the fiber. The two polarizers are rotated to make the polarization directions parallel or perpendicular.

Both the sample and the detection arm on which the lens and fiber are mounted can be rotated. To measure light scattered into different directions, we fix the sample and rotate only the detection arm [Fig. 2(a)]. The incident angle ϕ of white light is fixed at 0°, while the viewing angle changes. We also rotate the sample while fixing the detection arm [Fig. 2(b)]. The angle θ between the incident beam and de-

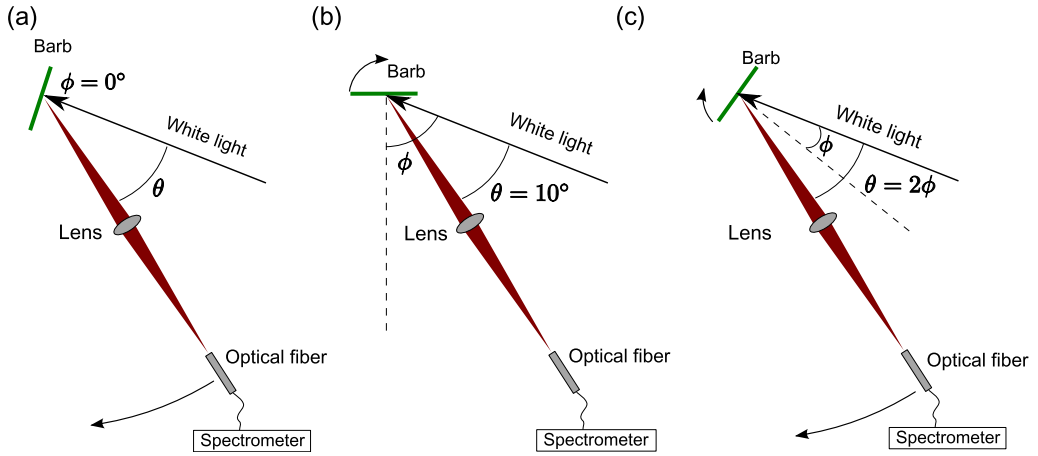

FIG. 2. (Color online) Schematics of optical setups for measurements of (a) angle-resolved scattering spectra, (b) nearly backward scattering spectra, and (c) specular reflection spectra of white light.

tection arm is kept at 10°, while the angle of incidence ϕ changes with sample rotation. The specular reflection is measured in the $\phi-2\phi$ geometry shown in Fig. 2(c). Namely, when the sample is rotated angle ϕ, the detection arm is rotated 2ϕ.

The cylindrical-shaped feather barbs are mounted horizontally so that their axes are perpendicular to the rotation axis of the goniometer. The apex and base of feather barbs are mounted on two separate holders while the probed parts in between do not have any substrate underneath (Fig. 3). Thus the effects of substrates are completely removed from the reflection and scattering data. The measured spectra of reflected or scattered light are normalized by the spectrum of incident light and then smoothed by convolution with a Gaussian function.

IV. POLARIZATION MEASUREMENT

The polarization experiment was done with the setup similar to the one shown in Fig. 2(a). The white light passes through a linear polarizer before it is incident onto the feather barbs. The incident angle $\phi=0°$. The detector collects the scattered light in the direction of angle θ from the surface normal. A linear polarizer is placed in front of the detector and the polarization direction can be changed. The incident beam and the detector form the scattering plane. If the polarization direction of light is parallel (or perpendicular) to the scattering plane, it is called p (or s) polarization.

We measured the spectra of scattered light whose polarization direction is either parallel or perpendicular to that of incident light. The former is called copolarization and the latter cross polarization. Figure 4(a) shows the spectra of co- and cross-polarized scattered light when the incident white light is p polarized and the scattering angle $\theta=10°$. The scattering spectrum of co-polarization $I_{co}(\lambda)$ has two peaks. The primary peak is at 534 nm and the secondary peak at 365 nm. In the scattering spectrum of cross-polarization $I_{cr}(\lambda)$, the primary peak disappears. The secondary peak remains, but its intensity is about 40% lower. Figure 4(b) is a plot of depolarization ratio $D_p(\lambda)=I_{cr}(\lambda)/I_{co}(\lambda)$. The two vertical lines mark the frequencies of primary peak and secondary peak. D_p reaches the minimal value of 0.08 at the frequency of primary peak. Hence, the primary peak is linearly polarized and its polarization equal to that of the incident light. $D_p=0.57$ at the frequency of the secondary peak, indicating

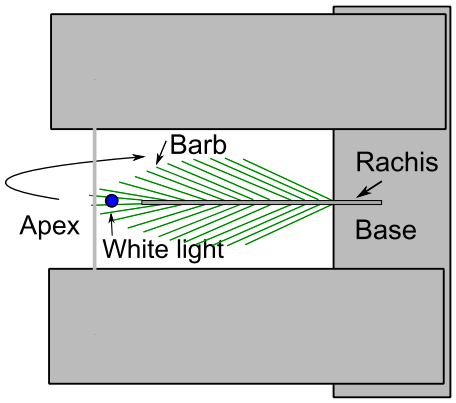

FIG. 3. (Color online) Schematic showing the orientation of feather barbs with respect to the rotation axis of goniometer, the location of incident light beam spot, and the way that the feather barbs are mounted to free the probed area from a substrate.

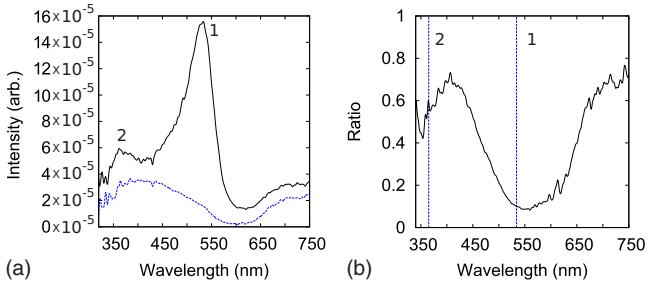

FIG. 4. (Color online) (a) Measured spectra of scattered light with copolarization (black solid curve) and cross polarization (blue dashed curve) when the incident white light is p polarized and the scattering angle $\theta=10°$. (b) depolarization ratio D_p versus wavelength λ. The vertical dashed lines mark the wavelengths of the primary peak (labeled 1) and the secondary peak (labeled 2).

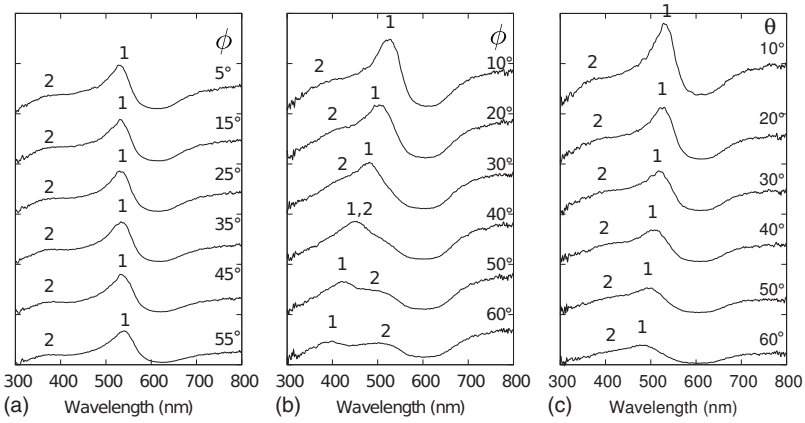

FIG. 5. Angular dispersions of the primary peak (labeled 1) and the secondary peak (labeled 2). (a) Measured spectra of light scattered to nearly backward direction of incident beam. The experimental setup is shown in Fig. 2(b). The angle θ between the incident beam and the detection direction is fixed at 10°. The incident angle ϕ is varied and the values are marked next to the curves. (b) Measured spectra of light reflected to the specular direction. The experimental setup is shown in Fig. 2(c). The values of incident angle ϕ are marked next to the curves. (c) Measured spectra of light being scattered to the directions other than the backward or the specular direction. The experimental setup is shown in Fig. 2(a). The incident light is normal to the sample surface. The sample does not rotate. The values of angle θ between the scattering direction and the surface normal are marked next to the curves.

the secondary peak is depolarized. However, D_p less than unity means the cross-polarization component is weaker than the copolarization one. Thus the memory of the polarization of the incident light is not completely lost. The maximal depolarization occurs at a frequency in between the primary and secondary peaks, which will be discussed later. Similar results are obtained when the incident light is *s*-polarized. These results confirm the primary peak is produced by single scattering, which does not change the polarization of light. The secondary peak is probably from multiple scattering which depolarizes light.

V. DIRECTIONAL PROPERTIES

In Ref. [13] we studied the angular dispersion of the primary peak. Here we investigated whether and how the secondary peak changes with the angles of observation and illumination as well as the sample orientation. First, we fix the direction of incident white light and the detector position [Fig. 2(b)]. The scattering direction is about 10° away from the incident beam (θ=10°), thus close to the backscattering direction. Figure 5(a) shows the measured spectra as the sample is rotated. The incident white light is unpolarized and there is no polarizer in front of the detector. Like the primary peak in the spectra, the secondary peak does not depend on the sample orientation. This result confirms the secondary peak is generated by the isotropic nanostructures in the feather barbs.

Then we conducted the specular reflection measurement using the setup in Fig. 2(c). Figure 5(b) shows the reflection spectra for different incident angle ϕ of (unpolarized) white light. As ϕ increases, the primary peak shifts to shorter wavelength, and the secondary peak to longer wavelength. The two peaks cross at ϕ between 30° and 40°. This experiment reveals the angular dispersion of the secondary peak is very different from that of the primary peak.

In addition to the backscattering and specular reflection, we also measured the spectra of light scattered into other directions with the setup in Fig. 2(a). With increasing θ, the primary peak blueshifts and the secondary peak redshifts [Fig. 5(c)]. A careful comparison to the data in Fig. 5(b) reveals that the scattering spectra for angle θ between the incident beam and the scattering direction resemble the reflection spectra of incident angle $\phi=\theta/2$. In the specular reflection experiment [Fig. 2(c)], the angle between the incident beam and the reflected beam is $\theta=2\phi$. Thus θ represents the angle between the incident beam and the line of sight in all three experimental setups in Fig. 2. The similarity between the scattering spectra and reflection spectra of the same θ implies the physical origins for light scattering and reflection from the quasiordered structures are identical. In the following we include specular reflection in the theoretical study of light scattering.

VI. SINGLE SCATTERING

In this section we simulate single scattering of light by the quasiordered structures before moving to double scattering in the next section. Let us consider light with an incident wave vector $\mathbf{k}_i$ being scattered to a wave vector $\mathbf{k}_o$. For elastic scattering, the magnitude of wave vector does not change. $|\mathbf{k}_i|=|\mathbf{k}_o|\equiv k=2\pi n_e/\lambda$, where n_e is the effective index of refraction and λ is the vacuum wavelength. Direction change of the wave vector is described by the scattering angle θ_m, as shown in Fig. 6(a). Such description is consistent with our experimental geometry. Note that θ in the experiments is the angle between the directions of illumination and observation *outside* the sample, and it is different from θ_m between $\mathbf{k}_i$ and $\mathbf{k}_o$ *inside* the sample due to light refraction at sample surface. The difference between $\mathbf{k}_i$ and $\mathbf{k}_o$ is equal to a spatial vector $\mathbf{q}$ of the structure, i.e., $\mathbf{k}_o-\mathbf{k}_i=\mathbf{q}$. From Fig. 6(b), we get

$$q=2k\cos(\theta_m/2). \tag{1}$$

Fourier power spectrum of a structure, $I(\mathbf{q})$, tells the spatial vectors exist in the structure and their strengths. SAXS di-

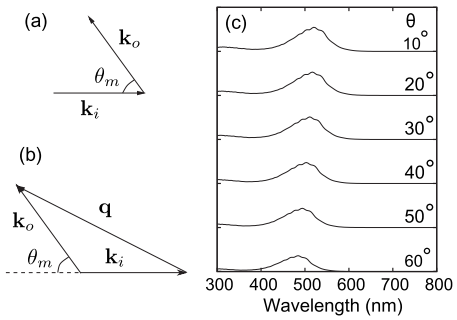

FIG. 6. (a) Schematic showing light with the incident wave vector $\mathbf{k}_i$ being scattered to $\mathbf{k}_o$. (b) Single-scattering diagram. $\mathbf{q}=\mathbf{k}_o-\mathbf{k}_i$ is a spatial vector of the structure. (c) Calculated single-scattering spectra for different scattering angles θ when the incident angle ϕ is fixed at 0°. The values of θ are marked next to the curves.

rectly measures $I(\mathbf{q})$. Since the quasiordered structures are isotropic, $I(\mathbf{q})$ is invariant with the direction of $\mathbf{q}$. It depends only on the magnitude $q \equiv |\mathbf{q}|$. As shown in Fig. 1(a), $I(q)$ is peaked at q_0, implying q is distributed around q_0.

From the measured optical scattering spectra, we calculated the q values for the primary peak and secondary peak using Eq. (1). Surface refraction of light is taken into account by computing θ_m from θ [20]. As shown in Fig. 7, the q value for the primary peak remains constant for different θ. It is equal to q_0 of the SAXS data if the effective index of refraction $n_e=1.25$. This value of n_e corresponds to 57% volume fraction of air, which matches the estimate from electron micrographs of the quasiordered structures. Therefore, the primary peak in the optical scattering spectrum originates from single scattering, i.e., light is scattered only once inside the nanostructure. The q value for the secondary peak changes with θ, indicating its origin is not single scattering.

We also compared the light scattering spectra to x-ray scattering spectra of feather barbs. In Fig. 1(a), the measured intensity of scattered light for $\theta=10°$ is plotted against q and overlaid with $I(q)$ from the SAXS data. While the primary peak of light scattering matches that of $I(q)$, the secondary peak has smaller q and higher amplitude than the second peak of $I(q)$. Hence, the secondary peak of light scattering is not related to the small second peak of $I(q)$.

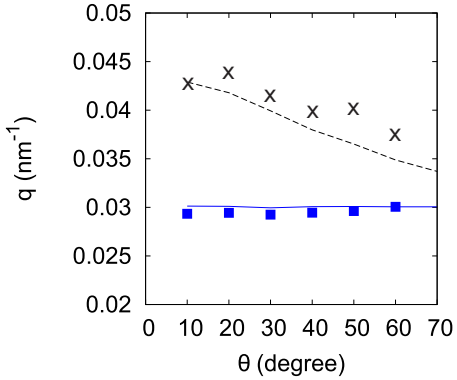

FIG. 7. (Color online) The values of $q=4\pi(n_e/\lambda)\cos(\theta_m/2)$ for the primary peak (squares, solid line) and secondary peak (crosses, dashed line) as a function of scattering angle θ. The symbols represent the experimental data and the lines the calculation results.

We calculated the single-scattering spectra using the Fourier power spectra of structure $I(\mathbf{q})$ from the SAXS data [Fig. 1(a)]. To eliminate the artificial signal from x-ray diffraction by the beam block in the center [inset of Fig. 1(a)], we fit the curve of $I(q)$ for smaller q [blue dashed line in Fig. 1(a)], and used the fitted result for light scattering calculation. The polarization of light is neglected in the calculation. For the single-scattering process, the probability of incident light with $\mathbf{k}_i$ being scattered to $\mathbf{k}_o$ is proportional to $I(\mathbf{q}=\mathbf{k}_o-\mathbf{k}_i)$. Thus the flux I_1 of scattered photons in a unit solid angle around θ_m is

$$I_1(k,\theta_m) = I(q)2\cos^2\left(\frac{\theta_m}{2}\right) = I\left[2k\cos\left(\frac{\theta_m}{2}\right)\right]2\cos^2\left(\frac{\theta_m}{2}\right). \tag{2}$$

The factor $2\cos^2(\theta_m/2)$ comes from the relation between k and q in Eq. (1). We integrate $I_1(k,\theta_m)$ over the experimental collection angle $\Delta\theta\sim5°$. Figure 6(c) plots the calculated spectra of scattered light in different directions when the incident beam is normal to the sample surface. In addition to the conversion of θ_m to θ, the reduction of scattered light intensity while exiting through the sample surface is taken into account. The calculated single-scattering spectrum has only one peak, which shifts to shorter wavelength at larger θ. The q value corresponding to the peak wavelength is plotted versus θ in Fig. 7 (blue solid curve) for comparison with the experimental data. The calculation result of single-scattering peak matches well with that of the primary peak in the measured scattering spectra.

VII. DOUBLE SCATTERING

Unlike the primary peak, the angular dispersion of the secondary peak in light scattering spectra does not follow that of the single-scattering peak. The polarization measurement suggests the secondary peak is from multiple scattering. The lowest order multiple scattering is double scattering, namely, the incident light is scattered successively twice before exiting the sample [21–26]. As shown schematically in Figs. 8(a) and 8(b), light is scattered from $\mathbf{k}_i$ to $\mathbf{k}_m$, and then from $\mathbf{k}_m$ to $\mathbf{k}_o$. The two successive scattering events are considered to be uncorrelated, and each is treated as single scattering. $\mathbf{k}_m-\mathbf{k}_i=\mathbf{q}_1$, and $\mathbf{k}_o-\mathbf{k}_m=\mathbf{q}_2$, where $\mathbf{q}_1$ and $\mathbf{q}_2$ are spatial vectors of the structure. Since scattering is elastic, $|\mathbf{k}_i|=|\mathbf{k}_m|=|\mathbf{k}_o|=k$.

Even when the directions of $\mathbf{k}_i$ and $\mathbf{k}_o$ are fixed, $\mathbf{k}_m$ can be in multiple directions. Figures 8(a) and 8(b) shows two scattering diagrams for the same $\mathbf{k}_i$ and $\mathbf{k}_o$ but different $\mathbf{k}_m$. α_1 and α_2 denote the angles for two successive single-scattering events. Since $I(q)$ of the quasiordered structure has a narrow distribution around q_0, the magnitudes of $\mathbf{q}_1$ and $\mathbf{q}_2$, i.e., q_1 and q_2, shall be close to q_0. As α_1 and α_2 increase, k must increase in order to keep q_1 and q_2 approximately equal to q_0. To illustrate the difference between single scattering and double scattering, let us assume $q_1=q_2=q_0$. For single scattering once the angle θ_m between $\mathbf{k}_i$ and $\mathbf{k}_o$ is fixed, the

wavelength λ or k is set by Eq. (1) with $q=q_0$. For double scattering, k does not have a unique value for a fixed θ_m. Instead there is a range of k corresponding to different directions of $\mathbf{k}_m$.

We calculated the double-scattering spectra directly from $I(\mathbf{q})$ without assuming $\mathbf{q}_1$ and $\mathbf{q}_2$ have the same magnitude q_0. Again the polarization of light is ignored in the calculation. The probability of incident light with $\mathbf{k}_i$ being scattered to $\mathbf{k}_m$ is proportional to $I(\mathbf{q}_1)=I(\mathbf{k}_m-\mathbf{k}_i)$, and the probability of successive scattering from $\mathbf{k}_m$ to $\mathbf{k}_o$ is proportional to $I(\mathbf{q}_2)=I(\mathbf{k}_o-\mathbf{k}_m)$. The summation of $I(\mathbf{q}_1)I(\mathbf{q}_2)$ over all possible directions of $\mathbf{k}_m$ gives the probability of incident light being scattered to direction θ_m. In the calculation we sampled 1000 directions of $\mathbf{k}_m$ which are uniformly distributed over 4π solid angle [27]. For comparison with the experimental data, we also took into account surface refraction of light and averaged the double-scattering spectra over 5° collection angle.

Figure 8(c) shows the calculated double-scattering spectra when the incident beam is normal to the sample surface $\phi=0°$. As θ increases, the double-scattering peak is broadened and split into two subpeaks. The subpeak at longer wavelength is stronger, and it shifts to longer wavelength with increasing θ. The broadening of the double-scattering peak can be understood qualitatively by approximating $I(q)$ as a delta function $\delta(q-q_0)$. When $\theta_m=0$, the single-scattering angles α_1 and α_2 can only be 90°. Thus only one wavelength is allowed for double scattering and it is equal to $\sqrt{2}\pi n_e/q_0$. As θ_m increases, α_1 and α_2 can take multiple values. The wavelength of double-scattered light is no longer unique for a fixed θ_m. At larger θ_m, the range of possible values for α_1 and α_2 is wider, thus the double-scattering spectrum becomes broader.

The maximal intensity at long wavelength side of the double-scattering spectrum can be explained by the angular dependence of single-scattering intensity. For a fixed θ_m between $\mathbf{k}_i$ and $\mathbf{k}_o$, the doubly scattered light at longer wavelength or smaller k results from single scatterings of smaller angles α_1 and α_2. According to Eq. (1),

$$\frac{dk}{d\alpha_{1,2}} = \frac{k}{2}\tan\left(\frac{\alpha_{1,2}}{2}\right), \tag{3}$$

when $q_1=q_2=q_0$. Thus k does not change much with α_1 or α_2 as long as α_1 and α_2 are small. Since the double-scattering intensity is proportional to the product of two single-scattering intensity integrated over α_1 and α_2, the smaller spectral shift of single-scattering peak with α_1 and α_2 at lower values of α_1 and α_2 give higher double-scattering intensity at longer λ.

Experimentally the efficiency of our detector decreases rapidly once the wavelength λ of light is shorter than 340 nm. Thus we could not resolve the subpeak at $\lambda<340$ nm in the double-scattering spectra. The secondary peak in the measured scattering spectra is mostly from the subpeak at longer wavelength of the calculated double-scattering spectra. In Fig. 7 we plot the value of $4\pi(n_e/\lambda)\cos(\theta_m/2)$ for this subpeak as a function θ (black dashed curve). The calculated angular dispersion agrees reasonably well with the experimental result (crosses), confirming the secondary peak originates from double scattering of light.

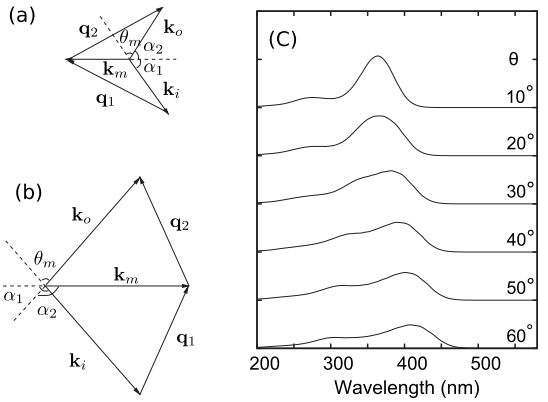

FIG. 8. (a) and (b) are schematics of double scattering. Light is scattered successively from $\mathbf{k}_i$ to $\mathbf{k}_m$, and then to $\mathbf{k}_o$. $\mathbf{q}_1=\mathbf{k}_m-\mathbf{k}_i$ and $\mathbf{q}_2=\mathbf{k}_o-\mathbf{k}_m$ are spatial vectors of the structure. The single-scattering angles α_1 and α_2 are smaller than 90° in (a) and larger than 90° in (b). (c) Calculated double-scattering spectra for different scattering angles θ when the incident angle ϕ is fixed at 0°. The values of θ are marked next to the curves.

VIII. DISCUSSION AND CONCLUSION

The secondary peak cannot be generated by the second-order scattering, which is described by scattering of the incident light from $\mathbf{k}_i$ to $\mathbf{k}_o$ by taking $\mathbf{q}_1$ and $\mathbf{q}_2$ simultaneously at the same position, $\mathbf{k}_o=\mathbf{k}_i+\mathbf{q}_1+\mathbf{q}_2$. This process does not have such a constraint $|\mathbf{k}_i+\mathbf{q}_1|=k$, which applies to the double scattering due to k conservation in each of two independent single-scattering events. Consequently the second-order scattering peak is much broader in frequency. For example, in the backward direction $\mathbf{k}_o=-\mathbf{k}_i$, with the approximation $I(q)\approx\delta(q-q_0)$, the value of k for the second-order scattering ranges from 0 and q_0. Hence, the second-order scattering spectrum spreads from $\lambda=280$ nm to infinity, completely different from the measured secondary peak in Fig. 4(a).

In conclusion, we investigated both experimentally and theoretically the secondary peak in optical scattering or reflection spectra of quasiordered nanostructures of bird feather barbs. The polarization measurement of scattered light illustrates that the secondary peak is depolarized while the primary peak maintains the polarization of incident light. The angle-resolved scattering or reflection spectrometry on feather barbs reveals the angular dispersion of the secondary peak is very different from that of the primary peak. Near the backscattering direction, the secondary peak has shorter wavelength than the primary peak. As the angle θ between the scattering direction and the incident beam increases, the secondary peak shifts to longer wavelength while the primary peak to shorter wavelength. At certain θ the two peaks cross.

We attributed the secondary peak to double scattering, i.e., light is scattered twice by the structure. The two successive scattering events are considered uncorrelated. From the

Fourier power spectra of quasiordered nanostructures measured with SAXS, we calculated both single-scattering and double-scattering spectra in various directions. The single-scattering spectrum exhibits one peak which corresponds to the dominant length of structural correlation. The double-scattering spectrum is broader, and splits into two subpeaks with increasing θ. The subpeak at longer wavelength redshifts as θ increases. Its angular dispersion reproduces that of the secondary peak observed experimentally. The agreement confirms the secondary peak originates from double scattering.

In addition to double scattering, our experimental data also provide a hint of triple scattering. In Fig. 4(b), the measured depolarization ratio of scattered light reaches the maximal value not at the frequency of the secondary peak, but in between the frequencies of the primary and secondary peaks. This may be due to triple scattering of light, which causes stronger depolarization than the double scattering. A qualitative analysis of triple scattering diagram shows that its spectrum is broader than that of double scattering. The frequency at which the triple scattering intensity is the highest is between that of single scattering and double scattering.

Finally we compare our results to the previous ones. There have been a series of studies on butterfly scales with single crystalline, polycrystalline, and amorphous photonic structures by measuring the spectrally and angularly resolved reflected and scattered light [28–30]. The optical reflectance spectra of the quasiordered structures can be explained by single scattering of light using the structural Fourier spectra [30]. In this study, we demonstrate that double scattering in a short-range ordered nanostructures produces additional peaks in the light scattering spectrum that contribute significantly to structural colors. This phenomenon has no analog in either periodic structures or random structures. In a perfectly ordered structure, multiple diffraction, or high-order diffraction does not create additional peaks, because a set of primary Bragg peaks would diffract into the same set of primary peaks. Vukusic *et al.* discovered colors being generated by double reflection from the concaved multilayers of butterfly wings [31]. The normally incident light, reflected from on one 45° inclined surface is directed across the concavity to the opposite orthogonal surface from where it returns parallel to the incident direction. This process strongly depends on the macroscopic geometry, and the direction of incident light. In contrast, the double-scattering phenomenon we report here originates from the intrinsic nanostructure with short-range order. It is insensitive to the surface profile, and exists for any direction of incident light. Therefore, the creation of additional spectral feature by double scattering is a unique property of short-range ordered structures, which has been widely utilized by nature for structural coloration.

ACKNOWLEDGMENTS

This work was supported with seed funding from the Yale NSF-MRSEC (Grant No. DMR-0520495) and NSF grants to H.C. (Grant No. EECS-0823345), E.R.D. (CBET), S.G.J.M. (DMR), and R.O.P. (DBI). Feather specimens were provided by the Yale Peabody Museum of Natural History and the University of Kansas Natural History Museum and Biodiversity Research Center. SAXS data were collected at Argonne National Laboratories with the help of Dr. Alec Sandy and Dr. Suresh Narayanan, and supported by the U.S. Department of Energy, Office of Science, Office of Basic Energy Sciences, under Contract No. DE-AC02-06CH11357.

[1] S. Kinoshita, S. Yoshioka, and J. Miyazaki, Rep. Prog. Phys. **71**, 076401 (2008).
[2] H. Ghiradella, J. Morphol. **202**, 69 (1989).
[3] P. Vukusic, J. R. Sambles, C. R. Lawrence, and R. J. Wootton, Proc. R. Soc. London, Ser. B **266**, 1403 (1999).
[4] R. O. Prum, *Bird Coloration* (Harvard University Press, Cambridge, MA, 2006), Vol. 1, pp. 295–353.
[5] S. Kinoshita and S. Yoshioka, ChemPhysChem **6**, 1442 (2005).
[6] J. Dyck, K. Dan. Vidensk. Selsk. Biol. Skrift. **18**, 5 (1971).
[7] J. Dyck, Z. Zellforsch Mikrosk Anat. **115**, 17 (1971).
[8] J. Dyck, in *Proceedings on International Ornithological Congress* (Australian Academy of Science, Canberra, 1976), Vol. 16, pp. 426–437.
[9] R. O. Prum, R. H. Torres, S. Williamson, and J. Dyck, Nature (London) **396**, 28 (1998).
[10] R. O. Prum, R. Torres, C. Kovach, S. Williamson, and S. M. Goodman, J. Exp. Biol. **202**, 3507 (1999).
[11] D. Osorio and A. D. Ham, J. Exp. Biol. **205**, 2017 (2002).
[12] E. R. Dufresne, H. Noh, V. Saranathan, S. G. J. Mochrie, H. Cao, and R. O. Prum, Soft Matter **5**, 1792 (2009).
[13] H. Noh, S. F. Liew, V. Saranathan, R. O. Prum, S. G. J. Mochrie, E. R. Dufresne, and H. Cao (to be published).
[14] P. Sheng, *Introduction to Wave Scattering, Localization, and Mesoscopic Phenomena* (Springer, Berlin; Heidelberg, 2006).
[15] *Waves and Imaging in Random Media*, edited by P. Sebbah (Kluwer Academic Publishers, Dordrecht, 2001).
[16] A. H. Brush, J. Protein Chem. **2**, 63 (1983).
[17] A. H. Brush, *Chem. Zool.* (Academic Press, New York, 1978), Vol. 10.
[18] R. O. Prum, E. R. Dufresne, T. Quinn, and K. Waters, J. R. Soc., Interface **6**, (Suppl 2), S253 (2009).
[19] M. Takenaka and T. Hashimoto, J. Chem. Phys. **96**, 6177 (1992).
[20] H. Noh, Ph.D. thesis, Northwestern University, 2009.
[21] D. W. Oxtoby and W. M. Gelbart, Phys. Rev. A **10**, 738 (1974).
[22] L. A. Reith and H. L. Swinney, Phys. Rev. A **12**, 1094 (1975).
[23] A. J. Bray and R. F. Chang, Phys. Rev. A **12**, 2594 (1975).
[24] H. Metiu, J. Chem. Phys. **68**, 1538 (1978).
[25] K. Hamano, N. Kuwahara, and M. Kaneko, Phys. Rev. A **21**, 1312 (1980).
[26] J. G. Shanks and J. V. Sengers, Phys. Rev. A **38**, 885 (1988).

[27] Source code can be downloaded at http://local.wasp.uwa.edu.au/pbourke/geometry/spherepoints

[28] K. Kertész, Z. Bálint, Z. Vértesy, G. I. Márk, V. Lousse, J. P. Vigneron, M. Rassart, and L. P. Biró, Phys. Rev. E **74**, 021922 (2006).

[29] D. G. Stavenga, H. L. Leertouwer, P. Pirih, and M. F. Wehling, Opt. Express **17**, 193 (2009).

[30] G. I. Márk, Z. Vértesy, K. Kertész, Z. Bálint, and L. P. Biró, Phys. Rev. E **80**, 051903 (2009).

[31] P. Vukusic and R. J. Sambles, Proc. SPIE **4438**, 85 (2001).